Dual Functional Roles of Lithium Oxide in Mixed Alkaline Earth Aluminosilicate Fiber Glasses

Hong Li, Daniel R. Neuville, Jincheng Du, Wenqing Xie

Dual Functional Roles of Lithium Oxide in Mixed Alkaline Earth Aluminosilicate Fiber Glasses

Hong Li[1]*, Daniel R. Neuville[2], Jincheng Du[3], Wenqing Xie[3]

[1.] Nippon Electric Glass, Shelby, NC, USA;

[2.] Université de Paris, IPGP-CNRS, Paris, France;

[3.] College of Engineering, University of North Texas, Denton, TX, USA

* lh412417@gmail.com

Abstract

Glass of MgO-CaO-Al_2O_3-SiO_2 system is one of the most focused research and development topics, such as for its wide applications of glass fiber reinforced compositions. The system potentially offers high mechanical properties, especially high fiber tensile modulus for ultralong wind turbine blades. However, challenges remain in processing technology because of its inherent high liquidus temperature. This study provided new insight into using Li_2O for improvement of fiber glass processing, lower melting/forming and lower liquidus temperature, plus added new benefit, i.e., increasing fiber modulus. The dual functionality of Li_2O in the glass was detailed in conjunction with Raman spectroscopic study aided by the curve deconvolution analysis, focusing on its influence on the speciation of glass structural groups in comparison with Na2O. Main findings from a separate study of MD simulations were also discussed to gain further insight of Li_2O roles in the glass network; for the first time, Li-induced higher coordination of aluminum-oxygen structures was revealed, which play a key factor in improving glass modulus.

Key words: lithium oxide, mixed alkaline earth aluminosilicate, speciation reaction of the network, high temperature properties, fiber sonic modulus.

Introduction

Continuous alkaline earth aluminosilicate glass fibers with and without boron have been widely used as reinforcements for plastic composite materials. E-Glass and E-CR glass fibers dominate the market applications, covering automotive, wind turbine blades, chemical storage tanks, pipes, printed circuit board substrate, infra-structure, etc.[1] Specialty glass fibers are those with less volume demanding, but exhibit unique properties to meet special application requirements, such as S-Glass fiber for aerospace and security protection with higher strength and higher modulus than E-Glass fiber. [1, 2] Fibers of R-Glass derivatives (such as products with trade name, H, INNOFIBER XM, TM, E8, etc. made globally) show significantly higher Young's modulus than E-Glass fiber, which are developed to meet OEM growing demands for longer wind turbine blade.[1, 3] The most recent development has shown fiber glass sonic modulus reached between 95 GPa and 106 GPa[4, 5]

S-Glass belongs to a ternary system of MgO-Al_2O_3-SiO_2 (MAS), whereas R-Glass, including its derivatives, falls into a quaternary system of MgO-CaO-Al_2O_3-SiO_2 (MCAS)[1-3] For renewable wind energy generation, most of commercial fiber glass development and production focus on R-Glass composition space with modifications by selectively introducing a small amount of other additives: monovalent oxide (Li_2O, Na_2O, K_2O), divalent oxide (SrO, BaO, ZnO), trivalent oxides oxide (B_2O_3, Y_2O_3, La_2O_3) and tetravalent oxides (TiO_2, ZrO_2) to optimize the chemistry for both processing and performance needs.[4-7]

To further reduce the cost of wind energy generation, a new generation of the wind turbine blades requires longer lengths as the energy generation is a function of the router's length squred.[8] Under the designed maximum wind pressure on the blade, to maintain the tip deflection the same between a longer blade and a shorter blade, higher fiber modulus is required. Typically

fiber glass offering significantly higher modulus contains significantly higher amount of Al_2O_3 and MgO but lower SiO_2.[1] As a result glass liquidus temperature (T_{Liq}) increases substantially, which becomes a challenging technical issue for fiber processing.[1,9] Fiber drawing temperature must be adjusted to a higher level to prevent the molten glass with higher T_{Liq} from devitrification; the formation of micro-scale crystals will lead to the fiber breakage during the drawing process and adversely impacts production yield, resulting in significant product cost increase. Another added production cost comes from a shorter service life of bushing operated at higher temperatures.

A study has been carried out earlier by one of the authors to examine the combined effect of introducing B_2O_3 and Li_2O at the expense of MgO on T_{Liq} and crystallization kinetics of the modified S-Glass (HS glass).[9] Significant T_{Liq} reduction of the HS glasses was achieved; one HS glass showed the reduction by 43^{o}C and another by 73^{o}C relative to 1425^{o}C reported T_{Liq} for S2 Glass®.[9] As a rule of thumb, fiber drawing temperature should be set at least 65^{o}C greater than T_{Liq}. The improved HS minimum fiber drawing temperature would be 1432^{o}C and 1402^{o}C, respectively, for the above cases according to the rule. However, T_{Liq} of both HS glasses are still too high to be used for a large commercial furnace production with an annual capacity of 20,000 MT or greater. In the study,[9] the combined effect of the modest substitution of MgO by B_2O_3 and Li_2O on T_{Liq} reduction did not reveal their individual composition effect.[9] Effects of mixed alkaline earth (MgO, CaO) on R-Glass liquidus temperature is nonlinear as reported in the literature.[3] Effects of rare earth oxide (RE_2O_3) on liquidus temperature and mechanical properties (fiber tensile strength and fiber sonic modulus) are also reported in the literature.[10] The studies reveal that the introduction of selective RE_2O_3 can reduce liquidus temperature and melt viscosity over a certain concentration level depending on their cation field strength,[10] plus

increases both fiber tensile strength and fiber sonic modulus at the same time.[10] While the introduction of Li_2O in glass is known to decrease melt viscosity,[11-13] to the best of our knowledge, a systematic study of effect of Li_2O on R-Glass is lacking in terms its effect on liquidus temperature and mechanical property relevant to the application of wind turbine blade. In the recent new R-Glass development, it has been discovered that Li_2O offers benefits on lowering both the melt viscosity and liquidus temperature, while improving fiber glass sonic modulus.[5] Being a network modifier, the incorporation of alkali oxides in silicate-based glasses generally decreases Young's modulus.[14, 15]

In this study, a baseline MCAS glass composition was modified by incorporating Li_2O at the expense of SiO_2 without changing other oxide ratios (only one exception) to investigate how Li_2O affects properties of glass melting and fiber drawing temperatures, liquidus temperature, and fiber sonic modulus. Raman spectroscopic study was also carried out to elucidate the effect of Li_2O on the polymerization of the glass network. Molecular dynamics (MD) simulations have also been carried out to gain further insight of the structural role of lithium ions in the network against sodium ions. The MD study has been reported separately;[16] this article focuses on the experimental structural characterization and mechanical property measurements; highlights of key MD simulation results will be provided in the discussion to enhance of interpretation of the experimental results of this study.

Experimental

Glasses of the designed compositions are shown in Table 1. With the increase in Li_2O, except for MCAS3 with the reduction of SiO_2 by increasing CaO and the removal of B_2O_3, the overall compositions of the glasses remain unchanged, i.e., the molar ratios of Al_2O_3/SiO_2, MgO/SiO_2,

and CaO/SiO_2 are kept at 0.25, 0.28, and 0.14, respectively (except for MCAS3 with CaO/SiO_2 of 0.22).

The glasses were prepared from batches, 1000 g each, and ingredients of the batches include clay, sand, limestone, magnesium oxide, colemanite, lithium carbonate, plus sodium carbonate in one case. Each batch was melted at 1500°C for 4h straight using a Pt/Rh crucible in an electrical furnace (Deltek). Each melt was poured onto a steel plat for cooling.

Table 1. Compositions (mol%) of MCAS glasses

ID	MCAS1	MCAS2	MCAS3	MCAS4	MCAS5	MCAS6	MCAS7	MCAS8
SiO_2	60.37	59.32	57.00	58.29	58.61	57.58	56.89	56.89
Al_2O_3	14.45	14.48	14.05	14.50	14.30	14.33	14.16	14.16
CaO	8.31	8.32	12.31	8.34	8.22	8.24	8.14	8.14
MgO	16.05	16.08	15.35	16.11	15.88	15.92	15.72	15.72
Li_2O	0.00	0.97	1.30	1.93	2.16	3.11	4.28	0.00
Na_2O	0.00	0.00	0.00	0.00	0.00	0.00	0.00	4.28
B_2O_3	0.83	0.83	0.00	0.83	0.82	0.82	0.81	0.81

*Compositions are converted from wt% of batch calculation using commercial batch sheet proven for accuracy within $\pm$ 0.3 wt% for SiO_2 (calibrated XRF method) and within $\pm$ 0.2 wt% for Al_2O_3, MgO, CaO, Na_2O, and B_2O_3 (calibrated XRF method) within $\pm$0.1 wt% for Li_2O (wet analysis).

Melt viscosity and liquidus temperature were measured using standard ASTM procedures, respectively.[17, 18] For the viscosity measurement, 500 g of glass cullet was feed to a Pt/Rh crucible and pre-equilibrated at 1450°C for 1h prior to the measurement from high temperature to low temperature. For the liquidus measurement, about 80 g of glass cullet with controlled particle size range was fed to a Pt/Rh boat and then inserted into a gradient temperature furnace (Orton).

XRD analysis of the phases formed in glass was selectively performed by using samples isothermally heat-treated at 1000°C for 20h, at which the samples show intense crystallization, i.e., becoming completely opaque. The sample selection was based on an initial sample screening

test by using FT-IR method, for which KBr sample disks were used for all treated samples. FT-IR method has been shown as a time effective means detecting crystal formation in the amorphous glass. PANalytical X'Pert diffractometer (Westborough, MA) was used with CuKα radiation under the following operating conditions: Cu-anode, 40kV/15mA, 0.04^o soller slits, 1^o divergence slit, and 0.10 mm receiving slit, the two-theta angle from 5^o to 60^o with 0.011^o per step and 18.87s per step. Phase analysis was aided by using commercial software (JADE®, Newtown Square, PA), based on the closest matching of the sample diffraction peaks with the reported phases from the ICDD database.

Fiber samples were manually prepared by using a fused silica rod to initiate a fiber from the molten glass in the Pt-crucible; the process is called fiber updrawing. Fiber diameter of the samples varied between 500 μm and 700 μm, over which the standard deviation of the measured sonic modulus is within 1% of the average value from 15 measurements, showing no bias to the fiber diameter variation. The fiber modulus (E_{fib}) was measured by using a sonic method; the procedure was detailed elsewhere.[19]

Raman spectroscopic measurements were carried out on Labram HR Evolution spectrometer equipped with a Peltier-cooled CCD and an 1800 lines per mm grating. The samples were excited with a Coherent MX 488,1 nm solid-state laser focused through a × 50 Olympus objective on the sample surface. The spectral resolution of the setup is ~1.2 cm^{-1} and the spatial resolution is ~1 μm through the confocal hole 50. 3 acquisitions of 60s per window were made and 3 windows are needed for the full spectra. The laser power was adjusted to 100 mW. Thanks to an ULF filter to attenuate laser signal, the Raman spectra were acquired from 20 to 1250 cm^{-1}.

The curve deconvolution of the Raman spectra was carried out using commercial software GRAMS AI (Galactic Industries Corp). Between 100 cm^{-1} and 1250 cm^{-1} wavenumber, the baseline correction was performed for each measured spectrum using a quartic function. The baseline corrected spectrum was then normalized relative to its maximum intensity of the band near 450 cm^{-1} prior to the curve fitting. The curve-fitting methodology was based on the nonlinear least-squares Levenberg-Marquardt method for fitting overlapping bands. Mysen et. al. [20] recommended the curve-fitting by minimizing overall χ^2 values defined as:

$$\chi^2 = \frac{1}{(n - f)} \sum_{i=1}^{n} \left(\frac{I_{i(m)} - I_{i(c)}}{R_{MSN}} \right)^2$$

where n is the number of data points in the fitted region, f is the total number of bands and baseline function parameters estimated from the Raman data (n-f is the number of "residual" degrees of freedom for the fit), $I_{i(m)}$ and $I_{i(c)}$ are the measured and calculated Raman intensity values for the i-th data point, respectively, and R_{MSN} is the estimated root mean squared noise in the measured data over the fitted region of the Raman spectrum, obtained by subtracting a smooth fit of the data from the raw data. The Levenberg-Marquardt algorithm iteratively adjusts parameters for each peak to minimize the χ^2-value. Based on literature reported studies, Raman bands between 100 cm^{-1} and 700 cm^{-1} represent several vibrational modes of the overall glass network, whereas Raman bands between 700 cm^{-1} and 1250 cm^{-1} represent vibrational modes of Q^n species of Si-O-Si network with different number (n) of the bridging oxygens (*BO*s) per SiO_4 tetrahedral unit for silicate glasses[21-24] and borate units for borosilicate glasses.[20-24] The deconvolution analysis of the spectra between 700 cm^{-1} and 1250 cm^{-1}. Five individual Gaussian bands were used in the curve-fitting without the restrictions of band position, width, and intensity.

3. Results

3.1 Glass properties

Table 2 summarizes the experimental results of the MCAS glasses, covering fiber density (ρ), fiber sonic modulus (E_{fib}), liquidus temperature (T_{Liq}), reference temperatures of glass melting (T_{10}) at 10 Pa·s viscosity and reference fiber drawing (T_{100}) at 100 Pa·s, ΔT between T_{100} and T_{Liq}, and crystalline phases of the selective heat-treated glasses from XRD analysis. In addition, the glass molar volume (V_M), atomic packing factor (APF), and basicity (*B*-value) are calculated based on the glass density, composition, and literature reported effective ionic radius[25] and basicity factor.[26, 27]

The addition of Li_2O slightly improves E_{fib} and at the same time decreases T_{10}, T_{100}, and T_{Liq}. The glass fiber density varied slightly between 2.581 and 2.596 g/cm^3 except slightly higher, 2.640 g/cm^3 for MCAS3 without B_2O_3 and slightly higher CaO.

Table 2. Measured properties of MCAS glasses along with the calculated physical parameters (in italic)

ID	MCAS1	MCAS2	MCAS3	MCAS4	MCAS5	MCAS6	MCAS7	MCAS8
ρ_{fib} (g/cm^3)	2.584	2.581	2.640	2.589	2.579	2.592	2.596	2.585
V_M (cm^3/mol)	*24.37*	*24.29*	***23.61***	*24.11*	*24.15*	*23.93*	*23.74*	***24.36***
APF	*0.432*	*0.433*	*0.441*	*0.435*	*0.434*	*0.437*	*0.439*	*0.435*
B-value	*0.552*	*0.555*	*0.568*	*0.558*	*0.558*	*0.561*	*0.564*	*0.567*
E_{fib} (GPa)	93.3	92.8	95.0	94.6	94.2	95.2	95.6	88.7
T_{Liq} (^{o}C)	1312	1268	1264	1240	1231	1203	1181	1255
T_{100} (^{o}C)	1301	N/A	1246	1239	1248	1212	1202	1253
ΔT (^{o}C)	*-11*	*N/A*	*-18*	*-1*	*17*	*9*	*21*	*-2*
$T_{drawing}$ (^{o}C)	*1362*	*1318*	*1314*	*1290*	*1281*	*1253*	*1231*	*1305*
T_{10} (^{o}C)	1480	N/A	1426	1425	1440	1400	1380	1449

Crystalline Phases (XRD)	An, In	N/A	N/A	N/A	An, Sp, In	An, Sp	An, Sp	An

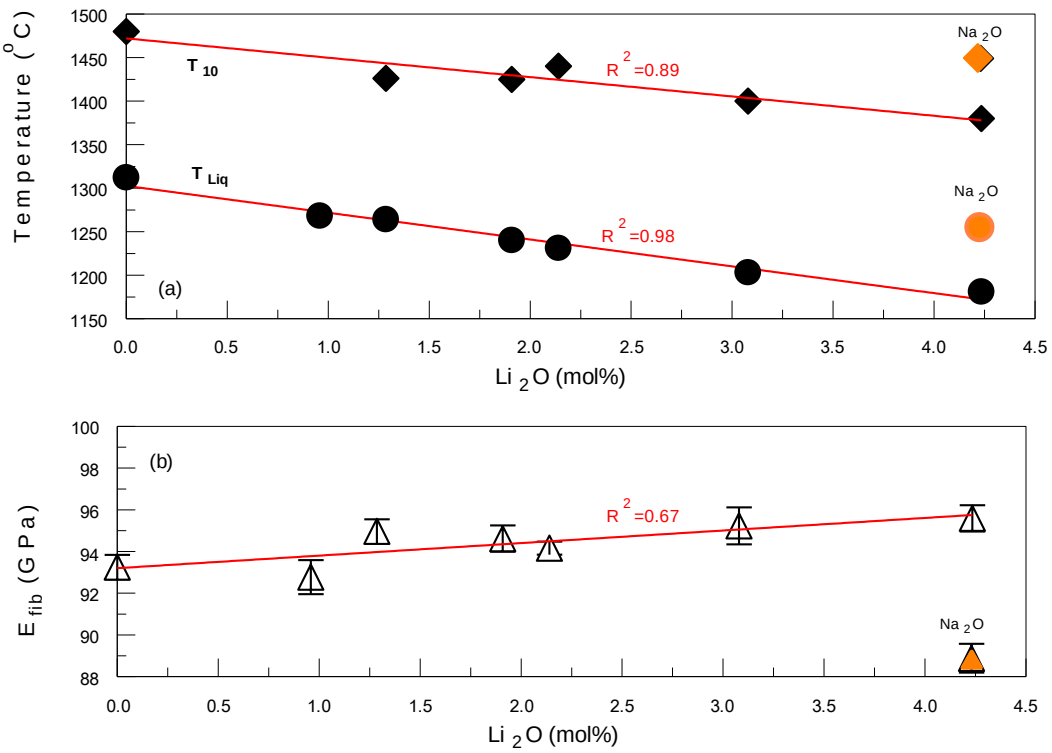

Fig. 1 Effects of Li_2O on (a) T_{Liq} and T_{10} and (b) E_{fib} where differences between Li_2O and Na_2O are compared.

Pending on the Li_2O content, a single or a mixture of two or three crystalline phases were found, namely anorthite ((Ca, Na)(Al, Si)$_4O_8$, ICDD 00-041-1481), β-spodumene ($LiAl(Si_2O_6)$, ICDD 01-071-2058), and Indialite ($Mg_2Si_5Al_4O_{18}$, ICDD 01-089-1485). The heat-treated baseline glass without Li_2O (MCAS1) contains anorthite ($CaAl_4Si_4O_8$) and indialite ($Mg_2Al_4Si_5O_{18}$). The heat treated MCAS7 containing the highest Li_2O exhibits only spodumene, whereas the heat treated Na_2O-containing glass (MCAS8) contains only anorthite. In addition, β-spodumene phase ($LiAlSi_2O_6$) are present in MCAS 5, 6 and 7 glasses after the heat-treatment, which contain Li_2O greater than 2 mol%. Three glasses (MCAS2, 3, 4) were not analyzed by XRD. Prior to the XRD analysis, all treated glass samples were scanned by using FTIR method (KBr pellet) as a quick

screen to determine whether the same crystalline phase(s) were present (see Fig. S1 in the supplementary information). The results show that these three glasses also contain anorthite and spodumene and hence, no XRD tests were carried out.

As depicted in Fig. 2, based on the intensity of the strongest X-ray diffraction peaks of the crystalline phases, indianite appears to be a dominant phase in MCAS1 without Li_2O. For MCAS5, 6, and 7 with Li_2O, spodumene phase is dominant. For MCAS8 with Na_2O replacement for Li_2O, anorthite phase is dominant.

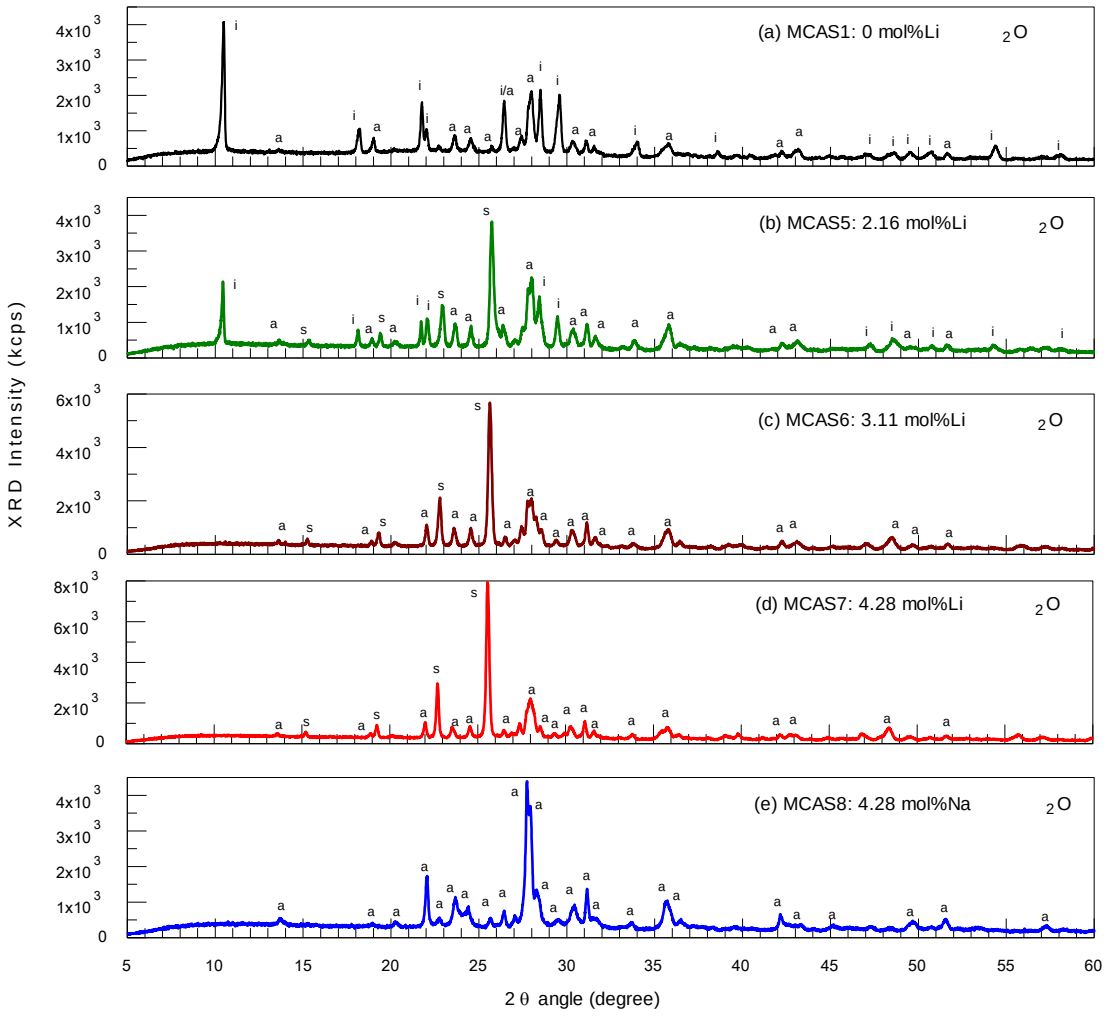

Fig. 2 XRD analysis of the heat-treated MCAS samples at 1000°C for 20h (a: anorthite, i: indialite, s: β spodumene).

The robustness of a fiber drawing process is qualitatively evaluated using a parameter, ΔT ($T_{100} - T_{Liq}$), which is typically between 65°C and 120°C for E-Glass with and without boron, pending on the glass composition.[1] For MCAS glasses of our study, ΔT is much narrow or even negative in some cases. Therefore, like S-Glass, a glass like S-Glass (MgO-Al_2O_3-SiO_2) should be drawn at a much higher temperature than T_{100}, i.e., $T_{drawing} \geq T_{Liq}+65^oC$. Tentatively, by this practical rule, the minimum $T_{drawing}$ values are tabulated in Table 2. In fact, in the preparation of samples for the sonic modulus measurements (E_{fib}) all fibers were drawn at approximately 1400°C to avoid crystal formation in the fibers.

3.2 Glass structure characterization

Fig. 3 depicts the experimental Raman spectra of the samples over the frequency between 10 cm^{-1} and 1250 cm^{-1}. A boson region exists between 10 cm^{-1} and 250 cm^{-1}, which contains information from a scattering continuum, the Raleigh tail of the exciting line, and a so-called boson peak (BP) according to literature.[28, 29] BP has been attributed to the excitations associated with rotational motions of the rigid SiO_4 tetrahedral units.[29, 30] For various silicate glasses investigated by using Raman scattering technique, Helhen et al.[30] proposed that BP increases in intensity and shifts to a higher frequency (or wavenumber) with the increase in the distortion of SiO_4 tetrahedra units. In our case, a small increase in intensity and a shift to high frequency with Li_2O content were observed (see an insert in Fig. 3), which can be explained by the decrease in silica content as Li_2O increases. It is noted that the frequency of the BP for the Na-glass (MCAS8) is much lower, which may be attributed to a mass effect of the alkali.

Between 150 cm^{-1} and 700 cm^{-1} the overall broad band represents the mixture of continuum contributions, predominantly Si-O-Si network vibration. For silica glass, previous studies show individual bands near 395 cm^{-1}, 460 cm^{-1}, 490 cm^{-1}, and 605 cm^{-1}. While 490 cm^{-1} and 605 cm^{-1} bands were assigned to oxygen vibrations of 4-membered and 6-membered, three-dimensional interconnected rings of SiO_4 tetrahedral units, respectively.[21,28] For the MCAS glasses with small amount of B_2O_3, besides predominant Si-O-Si-O-Si linkages in the network, significant portion of the Si-O-Al-O-Si linkages and a small portion of the Si-O-B-O-Si linkages are also expected, which will be discussed later.

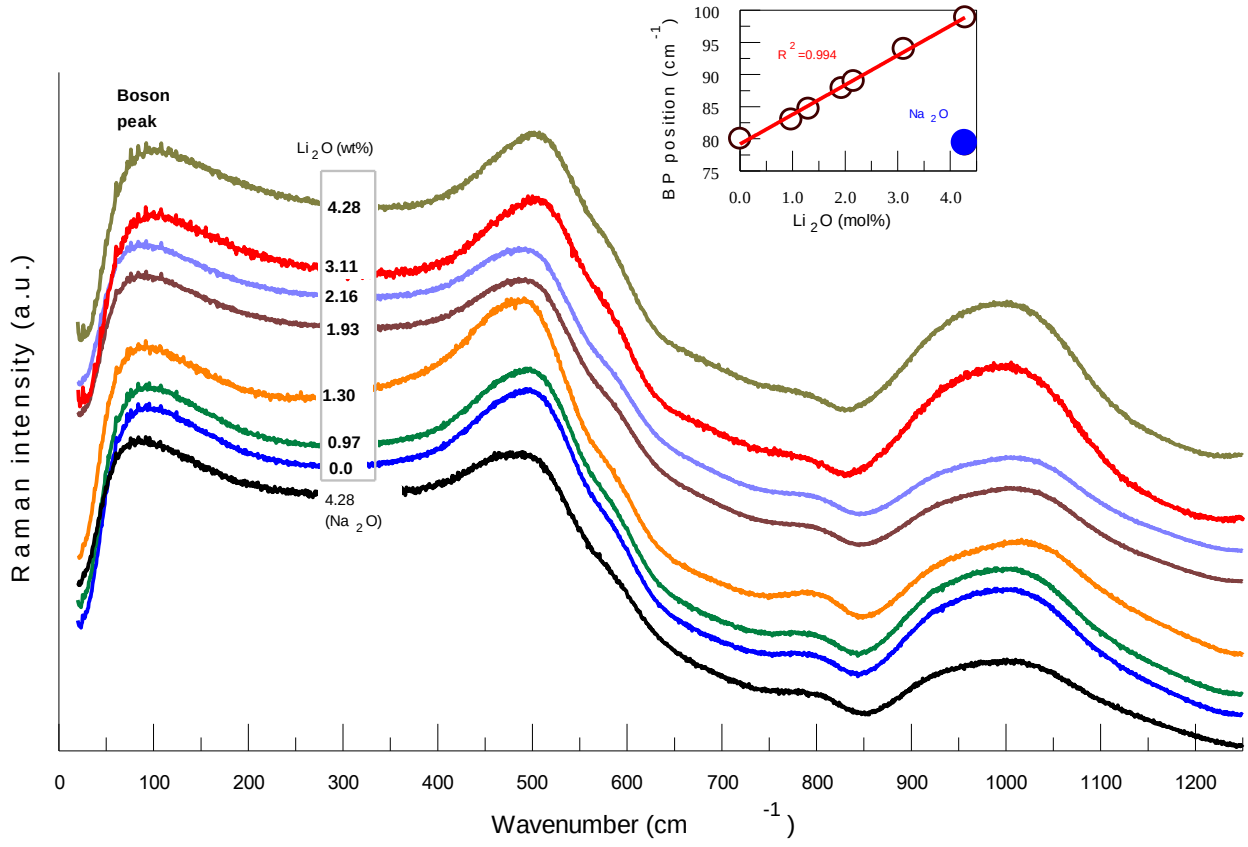

Fig. 3 Experimental Raman spectral data of the MCAS glasses with and without Li_2O (all spectra are vertically shifted for better clarity) and BP position as a function of Li_2O.

Between 700 cm^{-1} and 1250 cm^{-1}, the overall band near 1000 cm^{-1} appears to shift to a higher frequency initially as Li_2O increases and then returns to lower frequency with further

increase in the Li_2O content. The intensity of the weak band near 800 cm^{-1} decreases slightly and shifts towards lower frequency, including the Na-containing glass (MCAS8).

To further elucidate the glass structural response to Li_2O modification and any difference in the effects between Li_2O and Na_2O, the spectrum deconvolution analysis was carried out, focusing on the frequency range between 700 cm^{-1} and 1250 cm^{-1} where the distribution of the network structural groups, Q^n (n is the number of oxygens per SiO_4 unit), can be further resolved.

Fig. 4 depicts four examples of the deconvolution analysis of the Raman spectra, MCAS1 without Li_2O, MCAS3 with 1.30 mol%Li_2O, 4MCAS7 with 4.28 mol%Li_2O and MCAS8 with 4.28 mol%Na_2O substituting for Li_2O. The baseline of each spectrum was first corrected using a quartic function and then normalized by the maximum measured band intensity near 480 cm^{-1} using commercial software GRAMS AI. The curve fitting results (band position, p_k, and normalized band distribution, S_k, and goodness of the fit, χ^2) are summarized in Table 3. The curve fitting is satisfactory based on the low χ^2-values being less than 5.0, plus the random distribution of the narrow residues $\pm$0.02 unit between the fitted and measure spectrum values (not shown).

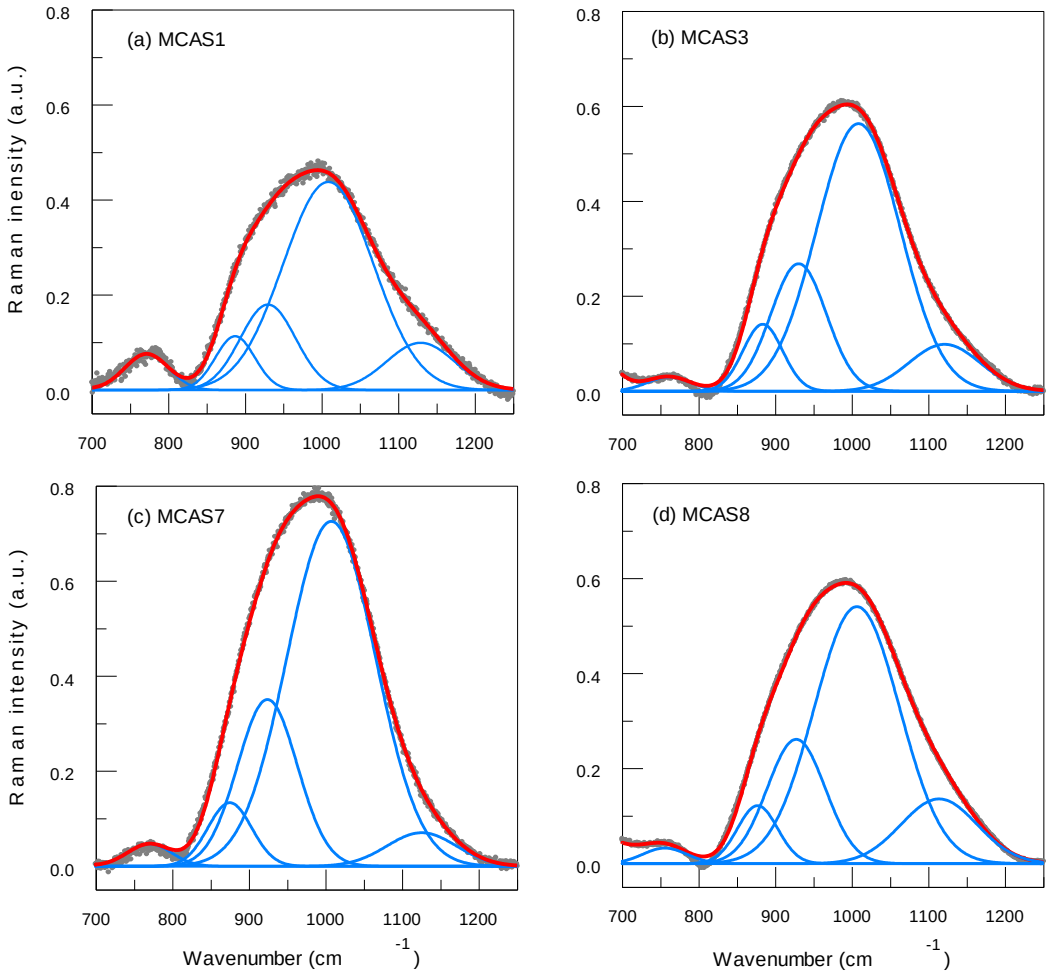

Fig. 4 Curve deconvolution of Raman spectra: (a) MCAS1, (b) MCAS3, (c) MCAS7, and (d) MCAS8.

Table 3. Results of Raman spectrum deconvolution analysis for MCAS glasses between 700 cm^{-1} and 1250 cm^{-1}

ID	Band position, p_k (cm^{-1})					Normalized band area, S_k (%)					Quality of fit χ^2
	p_1	p_2	p_3	p_4	p_5	S_1	S_2	S_3	S_4	S_5	
MCAS1	774	885	928	1006	1128	3.76	5.98	14.20	58.79	17.28	3.2
MCAS2	772	884	927	1008	1136	3.28	6.56	14.93	65.61	9.61	1.6
MCAS3	766	883	930	1008	1122	0.42	7.38	19.65	63.49	9.07	1.8
MCAS4	775	887	930	1015	1137	4.06	5.74	14.56	64.75	10.89	1.7
MCAS5	772	886	929	1013	1136	2.19	5.96	15.15	65.68	11.02	2.8
MCAS6	768	882	926	1011	1141	2.15	5.68	15.28	70.93	5.95	2.4
MCAS7	758	877	924	1007	1123	1.36	6.20	19.83	66.33	6.29	2.9
MCAS8	757	877	928	1008	1120	1.38	6.39	19.65	61.47	11.11	1.6

In general, the bands near 1128 and 885 cm^{-1} can be attributed to Q^4 and Q^2, respectively, both of which decrease with the Li_2O content. The band near 1006 cm^{-1} can be attributed to Q^3, shifting to a higher wavenumber, and increasing in area with the Li_2O content. The MCAS glass compositions of this study are too complex to determine the exact speciation reaction of Q^n species as will be detailed later. Over a certain Li_2O range, the reaction appears to follow the well-known silicate speciation reaction i.e., $Q^4 + Q^2 \Leftrightarrow 2Q^3$, proposed by Mysen.[21]

4. Discussion

4.1 Effects of Li_2O on glass properties

Overall, Li_2O/SiO_2 mole ratio increases from 0 to 0.075, whereas Al_2O_3/SiO_2, MgO/SiO_2, and CaO/SiO_2 remain unchanged at 0.25, 0.28, and 0.14, respectively, except for MCAS3 with CaO/SiO_2 of 0.22, plus the removal of B_2O_3. The viscosity response to Li_2O is linear and significant. In Table 2, glass molar volume (V_M) and atomic packing factor (APF) are deduced from the glass composition, density, and cation-oxygen distance,[25] The basicity value (B-value) was calculated based on the glass composition and optical basicity index of the oxides from the literature[26, 27] (cf. Table 2). It is apparent that Li_2O in the MCAS glasses decreases V_M, but increases both APF and B-value.

Fig. 6 depicts glass properties (T_{10}, T_{Liq}, E_{fib}) as a function of the molar volume occupied by cation-oxygen pairs, $V_{X\text{-}O}$ (equal to $V_M \cdot APF$), in the glass. Except for Na-containing glass (MCAS8) and boron-free glass (MCAS3), $V_{X\text{-}O}$ linearly decreases as Li_2O increases, implying the network "contraction" at higher Li_2O. For the Li-containing glasses with boron, T_{10} and T_{Liq} increase linearly with $V_{X\text{-}O}$. For the boron-free (MCAS3) and Na-containing glass (MACS8), the trend breaks down, implying the complexity of the glass network. Over the entire composition

range of our study, shown in Fig. 6c, E_{fib} can be well correlated with the second-order, polynomial function of V_{X-O}, i.e. $\alpha + \beta V_{X-O} + \gamma V_{X-O}^2$, with a linear regression coefficient, R^2-value, 0.95 (the Greek letters are fitting parameters). Should E_{fib} be singly correlated with APF or V_M (not shown), the discontinuity would appear, like T_{10} and T_{Liq} shown in Fig 6 (a&b).

Overall, the effects of Li_2O on the MCAS glass properties appear to be the same way as those of rare earth oxides (excluding Sc_2O_3) shown in Fig. S2 in the supplementary information. Both Li_2O and Y_2O_3 decrease T_{10} (as well as T_{100}, not shown) but increase E_{fib}.[10, 31] In terms of the Y_2O_3 effect on melt viscosity, the previous Raman study has confirmed its role in the glass network as a modifier.[10, 31] However, based on ^{27}Al MAS NMR measurements, Y_2O_3 induces the formation of five-coordinated AlO_5 units at the expense of AlO_4 units. In turn, the glasses exhibit higher fiber tensile strength and sonic modulus.[10,31]

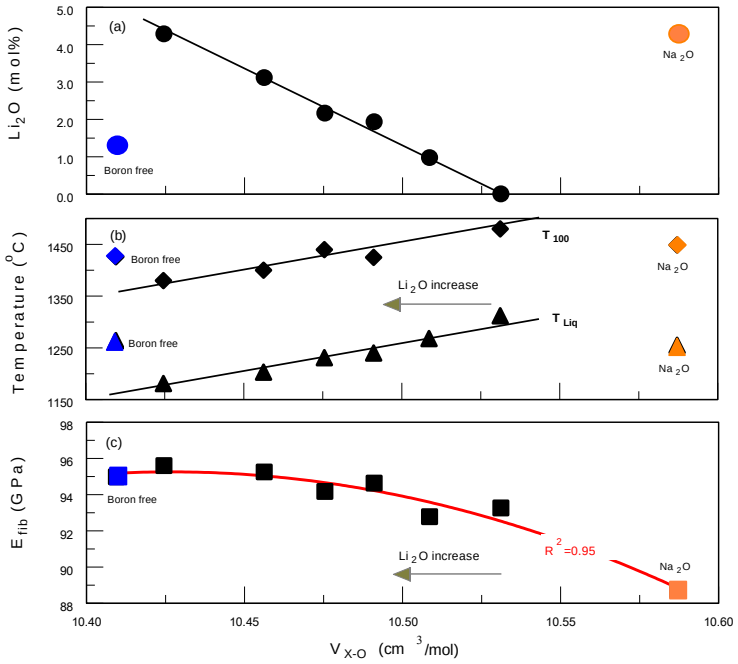

Fig. 6 Correlations between V_{X-O} and (a) Li_2O, (b) melting T_{10} and liquidus T_{Liq}, and (c) fiber sonic modulus E_{fib} (straight lines are shown for visual guides).

The effect of Li_2O on decreasing T_{Liq}, however, is not well understood. It may be reasoned by its effect on reducing activity of anorthite formation in the baseline (MCAS1). A previous study has shown that the partial replacement of Li_2O for Na_2O decreases the Na activity of the formation of nepheline ($NaAlSiO_4$) in the alkali-alkaline earth aluminoborosilicate glasses.[32] The opposite trends were also experimentally confirmed by either increase Na_2O or Al_2O_3 for the glass system.[32,33] As will be further discussed based on the recent MD simulations of the same set of the MCAS glass compositions, the glass network ring size can be increased by adding Li_2O, which may also decrease T_{Liq}.

Based on the XRD analysis of this study, Li_2O induces the formation of β-spodium ($LiAlSi_2O_6$) and in turn, lowers the activities of both Al_2O_3 and SiO_2 of the residual glass matrix and hinders the crystallization of the original phases of indianite ($Mg_2Si_5Al_4O_{18}$) and anorthite, (Ca, Na)(Al, $Si)_4O_8$. It should be noted that in the baseline and Li_2O containing glasses, Na_2O was not present and $Ca(Al, Si)_4O_8$ should be expected. For the MCAS8 containing Na_2O without Li_2O, anorthite chemistry should be closely matched with the standard phase (Ca, Na)(Al, $Si)_4O_8$. Indianite ($Mg_2Al_4Si_5O_{18}$) is considered as a secondary phase based on our study (i.e., much lower XRD intensity) shown in Fig. 2.

The finding on the positive effect of Li_2O on E_{fib} is surprising (cf. Fig 6a) as alkali cations are generally known for their adverse effects on glass mechanical properties of silicate-based glasses. Relative to the baseline MACS1 without Li_2O, MACS8 glass with 4.28mol%Na_2O exhibits significantly lower E_{fib} by 4.5 GPa, for example. However, MACS7 glass with 4.28 mol%Li_2O has higher E_{fib} by 2.3 GPa. The opposite response to the modification between Li_2O and Na_2O may be partially reasoned from their difference in cation field strength (CFS = Z/r^2 where Z is the valence and r is the effective ion radius): $Mg^{2+} > Ca^{2+} > Li^+ > Na^+$.[25] Although lithium belongs to the family of alkali group, its CFS is the highest among the alkali ions and even higher than Sr^{2+} and Ba^{2+}. The high CFS of lithium ions, plus smaller ionic size, makes it become a more attractive charge compensator, relative to Na^+ ion, to $[AlO_x]^{(3-2x/2)}$ anion groups (x = 4, 5, possibly 6). As will be discussed further, the MD simulations of the same glass set suggested the increase in AlO_5 units with Li_2O content.

4.2 Structural elucidation of Li_2O effect on the glass network

4.2.1 Raman spectroscopic findings

For the MACS glasses, as shown in Fig. 7, the PB band position increases with the Li_2O (cf. insert in Fig. 3), which is correlated with the decrease in T_{Liq} and T_{10} (as well as T_{100}), but the increase in E_{fib}. The effects of Li_2O on the glass network structure groups is detailed next.

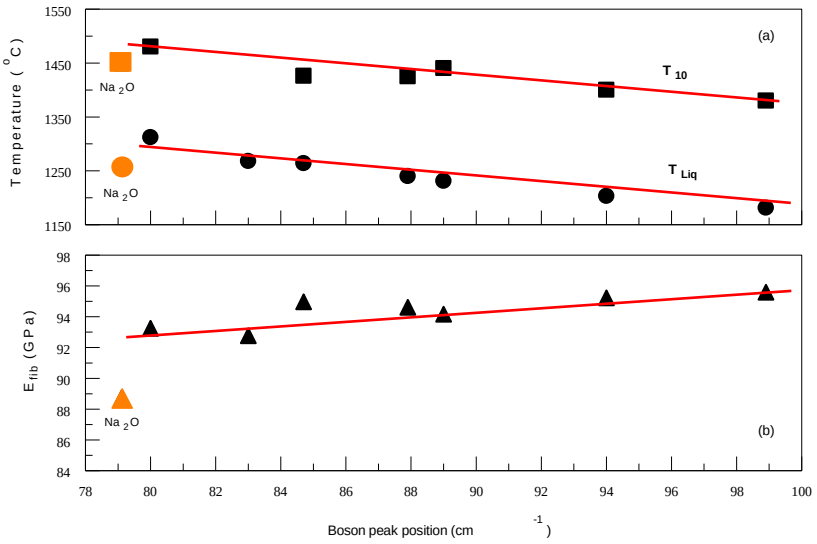

Fig. 7 Correlations of the Boson peak position with (a) melt property and (b) fiber sonic modulus (lines are provided for a visual guidance).

The spectrum deconvolution analysis (cf. Table 3) enables us to gain further insight in terms of the lithium effect on the averaged distribution of Q^n species.[21] For SiO_2 and M_xO_y-SiO_2 (M - alkalis or alkaline earths) silicate glasses, Raman bands centered between 1150 cm^{-1} and 1200 cm^{-1} are assigned to Q^4 (SiO_2), i.e., fully polymerized network, the band centered between 1050 cm^{-1} and 1100 cm^{-1} can be assigned to Q^3 ($Si_2O_5^{2-}$), band centered near 950 cm^{-1} can be assigned to Q^2 (SiO_3^{2-}), band centered near 900 cm^{-1} can be assigned to Q^1 ($Si_2O_7^{6-}$), and finally the band centered near 850 cm^{-1} to Q^0 (SiO_4^{4-}), i.e., a portion of the fully depolymerized network.[21] Specifically, between 200 cm^{-1} and 800 cm^{-1}, sodium disilicate glass exhibits a Raman band near 580 - 600 cm^{-1}, which was assigned to the mixed bending and stretching vibration of Si-O-Si groups in Q^3 groups. The mixed mode from Q^2 groups was also found, but shifted to 620 – 640

cm^{-1}, and further shifted to 700 cm^{-1} should Q^1 groups exist.[24] According to the literature, band centered near 1030 cm^{-1} belongs to the vibrational modes of different TO_4 units (T=Si, Al), which is named as T_2[3, 36, 37] and a band centered near 770 cm^{-1} is assigned to the B-O rings connected by one $[BO_4]$ and two $[BO_3]$ units, rather than deformation mode of δSi(Al)-O[36] because of the boron removal from MCAS3 (cf. Table 1) nearly eliminated the band (S_1 in Table 3) whereas Al_2O_3 in the glass is abundant (cf. Table 1).

From the Raman study, we observed the band near 1130 cm^{-1}, which corresponds to Q^4 (SiO_2), i.e., fully polymerized network. The band centered near 1006 cm-1 can be assigned to Q^3 ($Si_2O_5^{2-}$), band centered near 885 cm^{-1} may be assigned to Q^2 (SiO_3^{2-}), and finally the band centered near 774 cm^{-1} to borate units (BO_4). The band near 928 cm^{-1} may be characterized as the T2 peak vibration. The band centered around 1010 cm^{-1} can be attributed to a T2 asymmetric stretching vibration of the SiO_4 tetrahedron units.[34-37,39]

Fig. 8 depicts individual Raman band position (p_k) as a function of Li_2O. According to the tentative assignment of 770 cm^{-1} band, Li_2O appears to affect the borate local environment above 2 mol%, whereas the effect of Na_2O is the same as Li_2O (MCAS8). The same trend is held for Q^1 groups (cf. Fig. 8b), the 885 cm^{-1} band position remains stable till Li_2O is greater than 2 mol% and the substitution of Na_2O for Li_2O affects the band little, both near 875 cm^{-1}. For Q^2 groups, the band remains at 930 cm^{-1} with little change over Li_2O, including the substitution of Na_2O for Li_2O.

For Q^3 group, there appears a transition of its averaged environment; below 1.5 mol% Li_2O; the band slightly increases; further increase in Li_2O results in a step increase near 2 mol%Li_2O and followed by a linear decrease in the band position at higher Li_2O concentration (cf. Fig. 8c). The

boron removal with higher CaO and lower SiO_2 (MCAS3) or the substitution of Na_2O for Li_2O (MCAS8) seem to affect its environment little.

For Q^4 group, Li_2O in glass generally increases the band position from 1130 cm^{-1} to 1140 cm^{-1}; however, at 4.28 mol%Li_2O, the band position becomes significantly lower, even lower than the glass without Li_2O. The substitution of Na_2O for Li_2O further decreased the band position slightly. It is also noted that addition of CaO at the expense of SiO_2, plus boron removal, also results in the band position being significantly lower (cf. Fig. 8d).

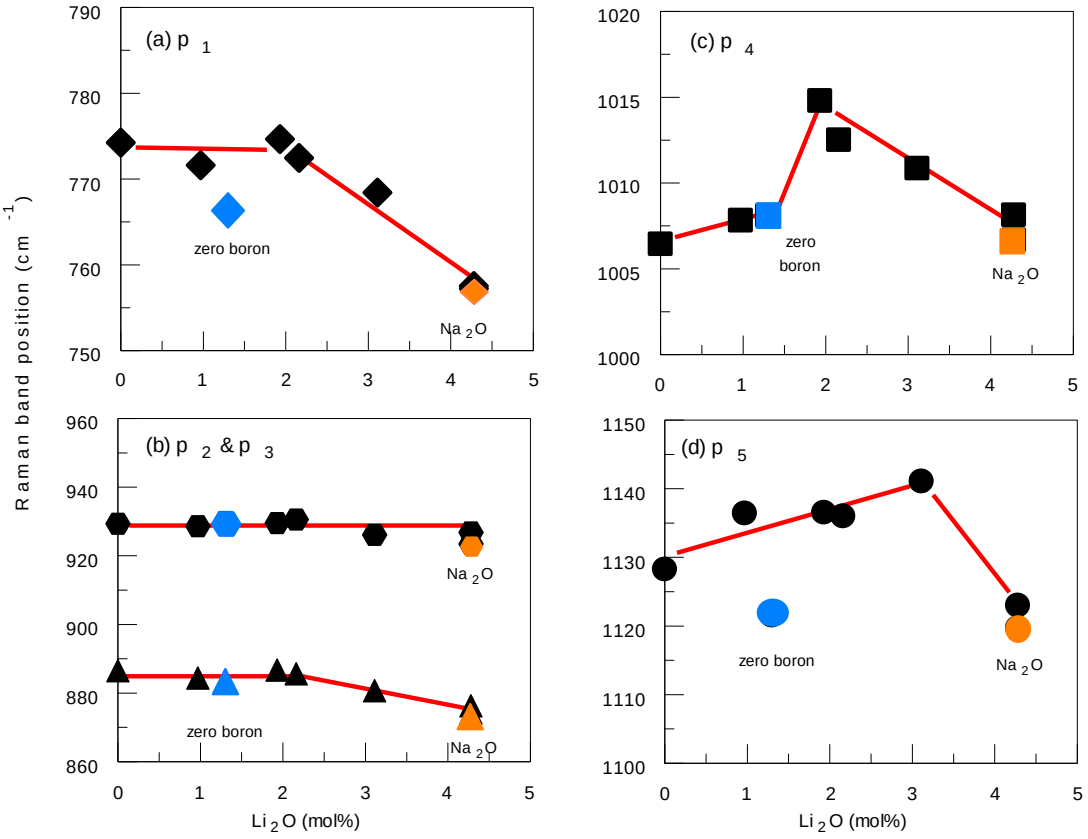

Fig. 8 Raman band position as a function of Li_2O (lines provided for a visual guidance)

Fig. 9 depicts the distribution of simulated Raman band areas (S_k) as a function of Li_2O. As Li_2O increases, S_1 near 770 cm^{-1} decreases linearly, implying a possible indication of the

reduction of BO_3 units as reported in the literature.[38-40] The substitution of Na_2O for Li_2O shows no difference in terms of the level of BO_3 reduction, which also agrees with the literature studies (cf. Fig. 9a). For MCAS3 without B_2O_3, the band area (S_1) without showing should be related to AlO_x instead.

The Q^1 group (S_2) near 885 cm^{-1} increases and Q^2 group (S_3) remains stable as Li_2O increases. Addition of CaO at the expense of SiO_2, plus boron removal, further increases Q^1 without any effect on Q^2. The substitution of Na_2O for Li_2O does not alter Q^1 and Q^2 (cf. Fig. 9b).

Below 4.28 mol% Li_2O, as shown in Fig. 8c&d, Q^3 group (S_4) increases at the expense of Q^4 group (S_5). At the highest Li_2O level, the Q^3 trend is reversed whereas Q^4 remains unchanged, implying that Li^+ ion likely function as a charge compensator to $[AlO_4]^-$ anion rather than the network breaker to create additional Q^3. Compared with Li_2O, the effect of Na_2O on the Q^3-Q^4 speciation is different, while S_4 (Q^3) and S_5(Q^4) decrease further.

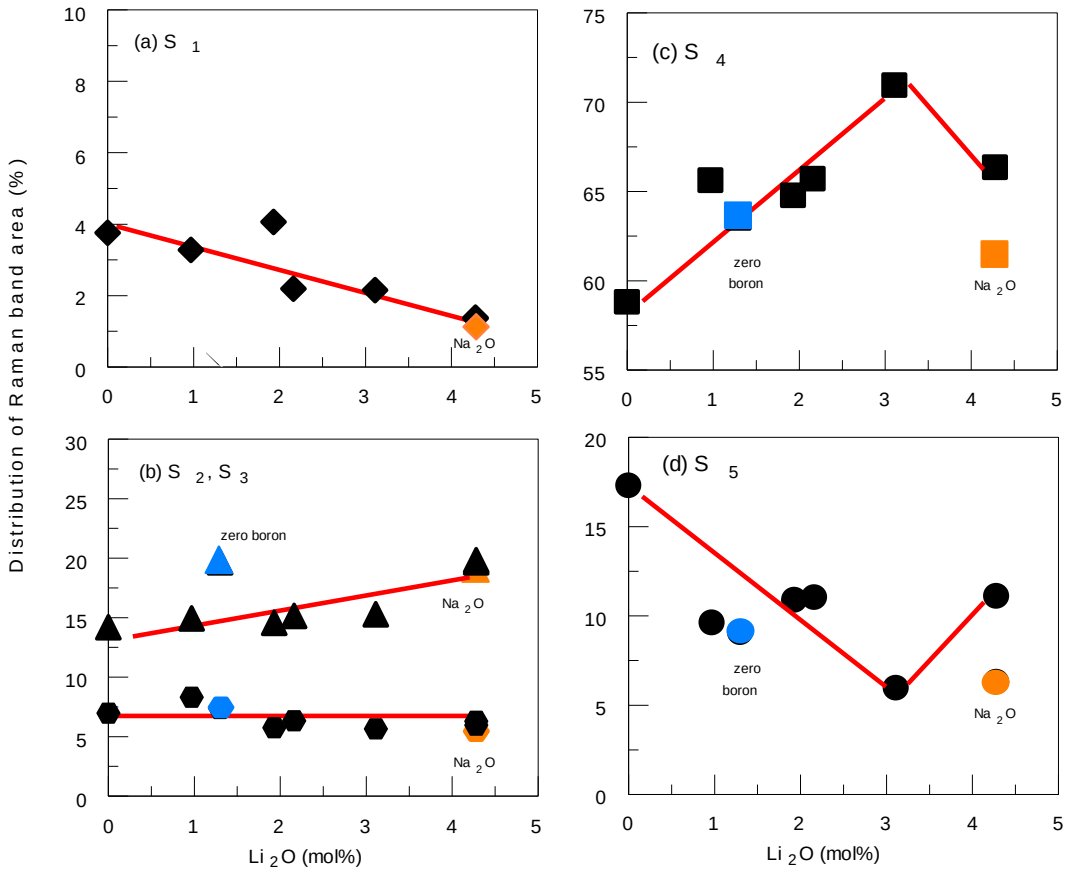

Fig. 9 Distribution of Raman band area as a function of Li_2O (lines provided for a visual guidance)

The Raman analysis provides evidence that Li_2O affects the glass network by increasing Q^1 and Q^3 at the expense of Q^4 as well as decreasing BO_3 units. The exceptional case is for MCAS7 with the highest Li_2O level, suggesting a possible interaction between Li_2O and Al_2O_3. From the MD simulation study, the interaction leads to the increase in five-fold coordinate AlO_5 units at the expense of four-coordinated AlO_4 units to be discussed later. At a similar level of Li_2O (MCAS3), the addition of CaO at the expense of SiO_2, plus boron removal, further increase Q^1 and decrease Q^4. The speciation reaction of Q^n groups derived from Raman spectroscopic study, i.e., increasing Q^1 and Q^3 at the expense of Q^4, supports the trend of melt viscosity or processing

temperatures (T_{10} and T_{100}) in response to Li_2O addition as well as Na_2O substitution for Li_2O. The effect of Li_2O on the suppressing liquidus temperature can also be related to the transformation of Q^4 species to Q^1 and Q^3 species. Specifically, the weakened glass connectivity, and the decrease of tri-/bridging oxygen have a positive effect on lowering glass liquidus temperature as suggested by MD simulation study discussed later.[17]

The increase in Q^3 and Q^1 groups at the expense of Q^4 groups lead to the increase in the glass modulus. Using SiO_2 glass as an example of a fully polymerized glass network with 100% Q^4 units, the glass has modulus 70 GPa. The glass network of E-Glass is composed of a mixture of Q^n groups from modifying SiO_2 glass by introducing primarily CaO and Al_2O_3 (CaO-Al_2O_3-SiO_2) with and without B_2O_3, plus $CaO/Al_2O_3 > 1$. The modified glass (E-Glass) exhibits a higher glass modulus, approximately 80 GPa. From Raman spectroscopic study, it appears that increase of both Q^1 and Q^3 at the expense of Q^4 can also increase fiber sonic modulus. The glass with the highest modulus (MCAS7) was achieved when the glass network contains the highest Q^1 and intermediate levels of Q^3 and Q^4, plus lowest level of BO_3. For the Na_2O substitution for Li_2O (MCAS8), the lowest fiber sonic modulus results; the glass network has the lowest amount of Q^3 plus Q^4.

4.2.2 Molecular dynamic simulations (MD) of Li_2O effect on the glass structures

A separate independent MD simulations study of the MACS glasses was performed by Xie, et. al.,[16] covering the same composition set used in this study. The MD based quantitative structure-property relationship (QSPR) analyses was detailed elsewhere.[16] At the cut-off distance ($d_{cut-off}$) of each cation-oxygen pair (M-O), the averaged coordination numbers (CN, $d_{cut-off}$) from the MD simulations over the composition range are as follows: CN(Si-O, 2.20 Å) = 4.00, CN(Al-O, 2.40 Å) = 4.01, CN(B-O, 1.85 Å) = 3.03, CN(Mg-O, 2.62 Å) = 4.05, CN(Ca-O, 3.20 Å) = 5.94-6.03, CN(Li-O, 2.48 Å) = 3.19-3.26, and CN(Na-O, 3.45 Å) = 6.23. It is evident that CN(Li-O) is

much smaller than CN(Na-O) due to ionic size difference. Similarly, CN(Mg-O) is also much smaller than CN(Ca-O) for the same reason. Furthermore, CN(Mg-O) is close to CN(Si-O) and CN(Al-O).

Beyond the averaged CN numbers, fine details of the speciation reactions for AlO_x and BO_x groups, respectively, were deduced from the MD simulations. Fig. 10a depicts the effect of Li_2O (and/or Na_2O) on the distributions of five-coordinated AlO_5 (at the expense of four-coordinated AlO_4) and four-coordinated BO_4 (at the expense of three-coordinated BO_3). The MD study suggested the possibility that the incorporation of Li_2O induces the formation of small amount of $[AlO_{5/2}]^{2-}$ at the expense of $[AlO_{4/2}]^-$ and $[BO_{4/2}]^-$ at the expense of BO_3.[17] On the other hand, the substitution of Na_2O for Li_2O substantially reduced $[AlO_{5/2}]^{2-}$, resulting in the increase in $[AlO_{4/2}]^-$ as expected based on other literature studies,[41, 42] and in turn, the decrease in BO_4; the latter implies that Na^+ ions primarily serve as a local charge compensator to $[AlO_{4/2}]^-$ anions to achieve the local electrical neutrality. Besides, Mg^{2+} ion, with much smaller size than Ca^{2+} ion and similar $CN_{(Mg-O)}$ as $CN_{(Al-O)}$, can serve as a charge compensator to $[AlO_{5/2}]^{2-}$, achieving the local electrical neutrality. As depicted in Fig. 10b, it is interesting that the effect of Li_2O on the formation of AlO_5 units is weaker by MD simulation yet resembles rare earth oxide (Y_2O_3) with higher field strength (AlO_5 in the latter case was measured by using ^{27}Al MAS NMR spectroscopic method).[10] Additional ^{27}Al MAS NMR spectroscopic study are considered to determine the distribution of AlO_4 - AlO_5 and BO_3-BO_4 as a function of Li_2O of the same MCAS glasses.

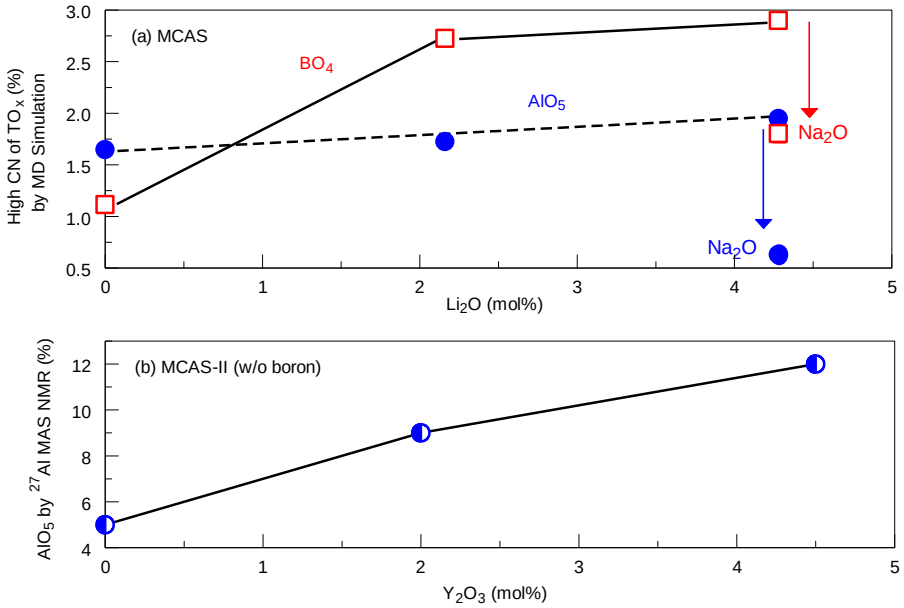

Fig. 10 Coordination of Al-O and/or B-O pairs: (a) estimation from MD simulations for low-boron MCAS glasses as a function of Li_2O and the substitution of Na_2O for Li_2O[17] and (b) ^{27}Al MAS NMR measurement for boron-free MCAS II glasses.[10]

The structure of the MCAS7 glass with the highest Li_2O is depicted in Fig. 10 where the detailed local structure is enlarged, revealing a tri-bridging oxygen with one five-fold coordinated AlO_5 and two 4-fold coordinated AlO_4 units, as well as a tri-bridging oxygen combined by one AlO_5 unit, one AlO_4 unit, and one SiO_4 unit. The dense-packed local area also shows a two-membered Al-O ring comprising edge-sharing AlO_5 and AlO_4 units.

The formation of [AlO_5] and [AlO_6] units at the expense of [AlO_4] units in alkaline earth aluminosilicate glasses have been well studied, [41,42] demonstrating Young's modulus increase when divalent cations of lower field strength are replaced by divalent cations of higher field strength. The same mechanism has been recently demonstrated for trivalent rare earth oxides modified aluminosilicate glasses.[7,10] The modified glasses were shown to contain higher [AlO_5] units at the expense of [AlO_4] units; in turn, exhibited both higher fiber sonic modulus and

higher fiber tensile strength.[7,10] To the best of our knowledge, it is the first time that the glass fiber sonic modulus increase by Li_2O is possibly linked with the formation of [AlO_5] units, more specifically, based on MD simulations,[16] the formation of try-oxygen structural units of one [AlO_5] unit connected with two [AlO_4] units and two [AlO_4] units, as well as a tri-bridging oxygen combined by one [AlO_5], one [AlO_4], and one [SiO_4]. The dense-packed local area also shows a two-membered Al-O ring comprising edge-sharing [AlO_5] and [AlO_4] units. With increase in BO_4 units at the expense of BO_3 units with higher Li_2O, it is also possible to make the glass higher in modulus. The separation of the contributions is not possible in this study; further study of the distributions of AlO_x and BO_x by ^{27}Al and ^{11}B MAS NMR spectroscopic method can further advance our insight.

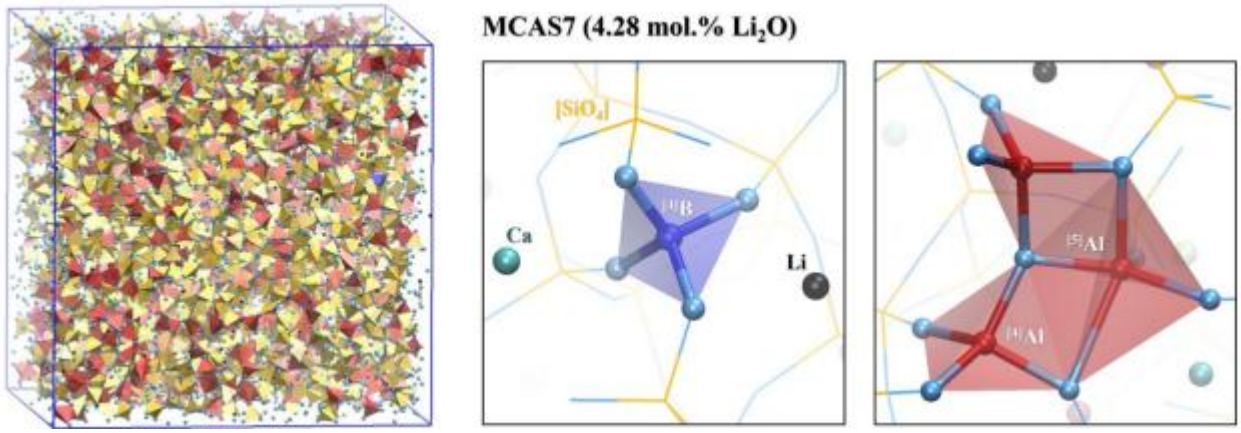

Fig. 11 MD simulation of the glass network structure and the local structure of try-oxygen structure around Al^{3+} with Li^+ ion surrounded.[16] (O-grey, Si-yellow, B-red, Al-blue, Mg-lime, Ca-cyan, Li-black.)

Comparing with the glass properties with other characteristic parameters from the MD simulations, such as the network (NT) connectivity and ring size, as depicted in Fig. 12, reveals that the melt viscosity (in terms of T_{100}) decreases with the reduction of the NT connectivity,

agreeing with the degree of the network polymerization. On the other hand, T_{Liq} decreases as the network ring size increases since the depolymerization of the network, i.e., reduction of NT connectivity, can increase T_{Liq} instead. Fiber sonic modulus (E_{fib}) is positively correlated with the network ring size and negatively correlated with the NT connectivity.

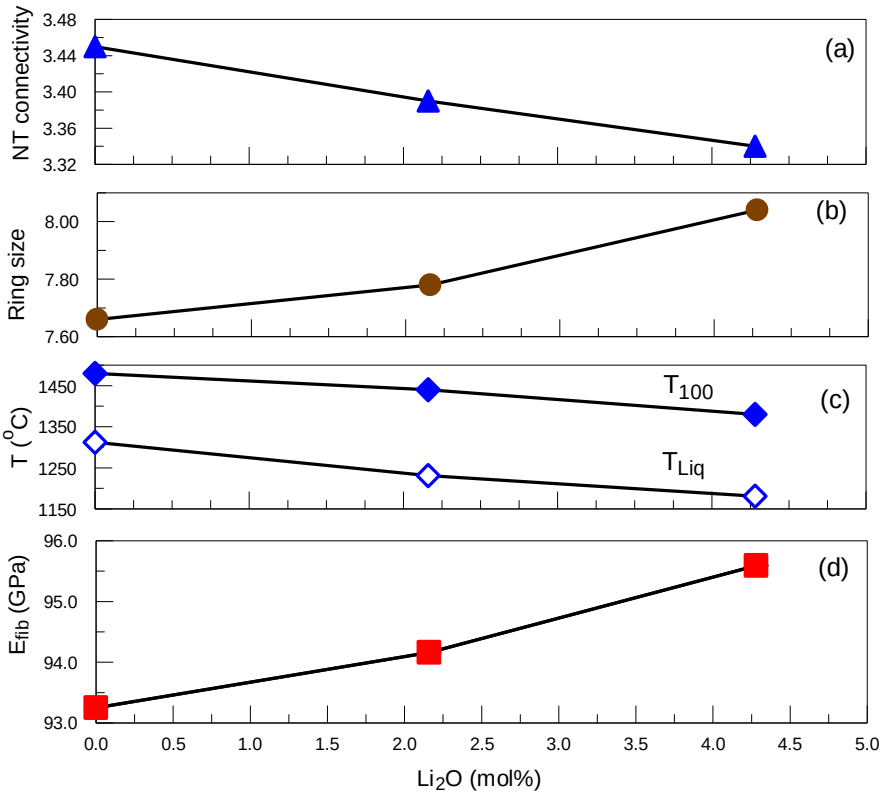

Fig. 12. Effects of Li_2O on (a) the MD derived network connectivity, (b) the MD derived network ring size, (c) measured melting and liquidus temperature, and (d) measured fiber sonic modulus.

5. Conclusion

A series of MgO-CaO-Al_2O_3-SiO_2 glasses were investigated to examine the effects of Li_2O on glass properties relevant to fiber glass processing (T_{10}, T_{100}, and T_{Liq}) and wind turbine blade application (fiber sonic modulus, E_{fib}). For the first time, the use of Li_2O was shown to improve both glass melting and fiber drawing processes and enhance glass fiber sonic modulus. The

effects can be generally correlated with the molar volume of cation-oxygen (V_{X-O}) of the glasses. Raman spectroscopic study of the MCAS glasses further shows the glass network weakening by Li_2O as a modifier, shifting the Boson peak to a higher position as the Li_2O content increases whereas the opposite change results by replacing Li_2O by Na_2O. The Raman deconvolution analysis revealed detailed glass structural group distribution, particularly the distribution of Q^3-Q^4 groups, which differs from the effect of Na_2O. Supporting data from a separate MD simulation study of the same set of glass compositions suggests that Li_2O potentially induce five-fold [AlO_5] units at the expense of four-fold [AlO_4] units and in turn, increase the oxygen packing density. The transformation of [AlO_4] to [AlO_5] can be one of the reasonings supporting the increase in fiber sonic modulus (E_{fib}), resembling the effect of rare earth oxide. Comparing with the changes of the network connectivity and ring size derived from the MD simulations, it can be also reasoned that the reduction of T_{Liq} by Li_2O is related to the decrease in the network connectivity and the increase in the network ring size in addition to the Li_2O effect on the activity of crystalline phases, anorthite vs β-spodumene. Additional ^{27}Al MAS NMR spectroscopic study is considered to determine the distribution of AlO_4 - AlO_5 and BO_3 – BO_4 as a function of Li_2O for the same MCAS glasses.

Reference (to be completed)

[1] Zu Q, Solvang M, Li H. Commercial glass fibers. In: Li H, editor. Fiberglass Science and Technology: Chemistry, Processing, Characterization, Application and Sustainability. Gewerbestrasse: Springer; **2021**. pp.1-88.

[2] Hausrath RH, Longobardo AV. *High-Strength Glass Fibers and Markets*. In: Wallengerger FT, Bingham PA, editors. Fiberglass and Glass Technology. New York: Springer; **2010**. p.197-225

[3] Li H, Demirok G, Atilgan S, Vennam S, Charpentier T. High-modulus glass fiber for wind renewable energy generation: Selective review on the recent research and development. J. Int. Appl. Glass Sci. 2024; 1-4. https://doi.org/10.1111/ijag.16672

4. H, Li, GLASS COMPOSITIONS, FIBERIZABLE GLASS COMPOSITIONS, AND GLASS FIBERS MADE THEREFROM, EP 3022163B1, Electric Glass Fiber America LLC (July 7, 2021)

5. H. Li, Glass compositions, Fiberizable Glass Compositions, and Glass Fiber Made Therefrom, US 2023/0133178A1 Electric Glass Fiber America, LLC (May 4, 2023).

6. R. Hausrath, A. Longobardo, and B. Rupple, "High Modulus Glass Fibers," WO 2014/062715A1, AGY Holding Corp. (April 24, 2014)

7. H. Li, P. Westbrook, "Glass Compositions, Fiberizable Glass Compositions, and Glass Fibers Made Therefrom," US 9278883 B2, PPG Industries Ohio, Inc. (March 8, 2016).

8. R&D Pathways for Supersized Wind Turbine Blades, Report No. 10080081-HOU-R-01 Lawrence Berkeley National Laboratory (March 7, 2019)

[9] Zu Q, Huang SX, Zhang Y, Huang SL, Liu JS, Li H. Compositional effects on mechanical properties, viscosity, and crystallization of (Li_2O, B_2O_3, MgO)-Al_2O_3-SiO_2 glasses, *J. Alloys & Comp.* 2017, 728: 552-563.

[10] Charpentier T, Ollier N Li H. RE_2O_3-alkaline earth-aluminosilicate fiber glasses: Studies of melt properties, crystallization, and network structures. *J. Non-Crystalline Solids*. **2018**, 492: 15–125.

[11] Fluegel A. Glass viscosity calculation based on a global statistical modeling approach. *Glass Technol.* **2007**, 48:13-30.

[12] Yang K, Zheng WH, Cheng JS. Effect of Li_2O on viscosity and thermal expansion of silicate glass. *Adv. Mater. Res.* 2011

[13] Chen LF, Liu K, Han P, Yang B, Feng LH. Effects of Li_2O on structure and viscosity of CaO-Al_2O_3-based mold fluxes. *J. Chem.* **2021**, 1-8, doi.org/10.1155/2021/6674453

[14] Volf MB. Mathematical Approach to Glass. New York: Elsevier, **1988**.

[15] Weigel C, Le Losq C, Vialla R, Dupas C, Clément S, Neuville DR, Rufflé B. "Elastic moduli of $XAlSiO_4$ aluminosilicate glasses: effects of charge-balancing cations. *J. Non-Cryst. Solids*. 2016, 447:267-272.

[16] Xie WQ, Li H, Neuville DR, Du JC. Structure-property relationships of mixed alkaline earth, low-boron aluminosilicate fiber glasses from molecular dynamics simulations and QSPR analysis. *J. Am. Ceram. Soc.* **2024**, x: xx-xx.

[17] Standard Practice for Measuring Viscosity of Glass Above the Softening Point. C965-96, Annual Book of ASTM Standards, ASTM, 2012.

[18] Standard Practices for Measurement of Liquidus Temperature of Glass by the Gradient Furnace Method. C829 -81, Annual Book of ASTM Standards, ASTM, 2010

[19] Li H, Richards C, Watson J. High performance glass fiber development for composite applications. *Int. J. Appl. Glass Sci.* 2014, 5: 65-81.

[20] Mysen BO, Finger LW, Virgo D. Curve-fitting of Raman spectra of silicate glasses. *Amer. Mineral.* **1982**, 67:686-695.

[21] Mysen BO. Structure and properties of silicate melts. New York: Elsevier, 1988, pp. 354

[22] Mysen BO, Virgo D, Seifert FA. Relationships between properties and structure of aluminosilicate melts. *Am. Mineral.* **1985**, 70: 88-105.

[23] McMillan P, Piriou B, Navrotsky A. A Raman spectroscopic study of glasses along the joints silica-calcium aluminate, silica-sodium aluminate, and silica-potassium aluminate. *Geochim. Cosmochim. Acta*. **1982**, 46: 2021-2037.

[24] Seifert FA, Mysen BO, Virgo D. Three-dimensional network structure of quenched melts (glass) in the system SiO_2-$NaAlO_2$-SiO_2-$CaAl_2O_4$ and SiO_2-$MgAlO_4$. *Am. Mineral.* **1982**, 67: 696-717.

[25] Shannon RD, Prewitt CT. Effective ionic radii in oxides and fluorides. Acta Cryst. 1969, B25: 925-946.

[26] Duffy JA, Ingram MD. Interpretation of glass chemistry in terms of the optical concept. J. Non-Cryst. Solids. 1976, 21: 373-410.

[27] Duffy JA. 2002. "The Electronic Polarisability of Oxygen in Glass and the Effect of Composition. J. Non-Cryst. Solids. 2002, 297: 275-284.

[28] Malinovsky VK, Sokolov AP., 1986. The nature of boson peak in Raman scattering in glasses. Solid State Comm. 1986, 57: 757–761.

[29] Buchenau U, Prager M, Nücker N, Dianoux AJ, Ahmad, N, Phillips WA. Low-frequency modes in vitreous silica. Phys. Rev. 1986, B 34: 5665–5673.

[30] Hehlen B, Courtens E, Yamanka A, Inoue K. Nature of the boson peak of silica glasses from hyper-Raman scattering. J. Non-Cryst. Solids. 2002, 307: 185–190.

[31] Li H, Charpentier T, Du JC, Vennam S. Composite reinforcement: Recent development of continuous glass fibers, Int. J. Appl. Glass Sci. 2017, 8: 23 – 36.

[32] Li H, Jones B, Hrma P, Vienna J. Composition effect on liquidus temperature of high-level waste glasses precipitating nepheline. Peeler DK, Marra CD, eds. *Ceram. Trans*. **1997**, 87: 279-288

[33] Li H, Hrma P, Vienna JD, Qian M, Su Y, D.E. Smith DE. Effects of Al_2O_3, B_2O_3, Na_2O, and SiO_2 on nepheline formation in borosilicate glasses: Physical and chemical correlations. J. Non-Cryst. Solids. 2003, 331: 202 – 216.

[34] Sharma SK, Simons B, Yoder HS Jr. Raman study of anorthite, calcium Tschermak's pyroxene, and gehlenite in crystalline and glassy states. *Am. Mineral.* **1983**, 68: 1113-1125.

[35] Le Losq C, Neuville DR. Effect of the Na/K mixing on the structure and the rheology of tectosilicate silica-rich melts," *Chem. Geology*. **2013**, 346**:** 57-71.

[36] Muller W, Hafnert M, Reich P, Brzezinka KW. Raman spectroscopic investigation of the system $CaO/Al_2O_3/SiO_2$. *Cryst. Res. Technol*. **1983**, 18: K49-K52.

[37] McMillan P. A Raman spectroscopic study of glass in the system $CaO\text{-}MgO\text{-}SiO_2$. *Am. Mineral.* **1984**, 69: 645-659.

[38] Hayek R EI, Ferey F, Florian P, Pisch A Neuville DR. Structure and properties of lime alumino-borate glasses. *Chem. Geo.* 2017, 461: 75-81.

[39] Yano T, Kunimine N, Shibata S, Yamane M. Structural investigation of sodium borate glasses and melts by Raman spectroscopy. I. Quantitative evaluation of structural units. *J. Non-Cryst. Solids*. 2003, 321: 137-146.

[40] Osipov, AA, Osipova LM. Structure of lithium borate glasses and melts: investigation by high temperature Raman spectroscopy. *Phys. Chem. Glasses: Eur. J. Glass Sci. Technol. B.* **2009**, 50: 343–354.

[41] Philipps K, Stoffel RP, Dronskowski R, Conradt R. Experimental and theoretical investigation of the elastic moduli of silicate glasses and crystals. *Frontiers Mater*. **2017**, 4 https://doi.org/10.3389/fmats.2017.00002

[42] Weigel C, Le Losq C, Vialla R, Dupas C, Clement S, Neuville D R, Ruffle B. Elastic moduli of $XAlSiO_4$ aluminosilicate glasses: effects of charge-balancing cations. *J. Non-Cryst. Solids*. **2016**, 447: 267-272.

Supplement Information

Dual Functional Roles of Lithium Oxide in Mixed Alkaline Earth Aluminosilicate Fiber Glasses

Hong Li[1]*, Daniel R. Neuville[2], Jincheng Du[3], Wenqing Xie[3], Stephen Bright[1]

[1.] Nippon Electric Glass, Shelby, NC, USA;

[2.] Université de Paris, IPGP-CNRS, Paris, France;

[3.] College of Engineering, University of North Texas, Denton, TX, USA

Based on FT-IR pre-screening test shown in Fig.2, one of the crystalline phases matches closely with natural anorthite (An)[28] and to a great degree, some of the IR bands also matched with IR bands of β-spodumene (Sp) reported in the literature.[29] Based on the FTIR results showing all treated samples exhibiting similar crystalline phases, therefore, the heat-treated glass samples were selectively examined by using XRD method and the results are depicted in Fig. 3 as well as summarized in Table 2. Both anorthite and β-spodumene phases suggested by IR tests are confirmed by XRD analysis as discussed next.

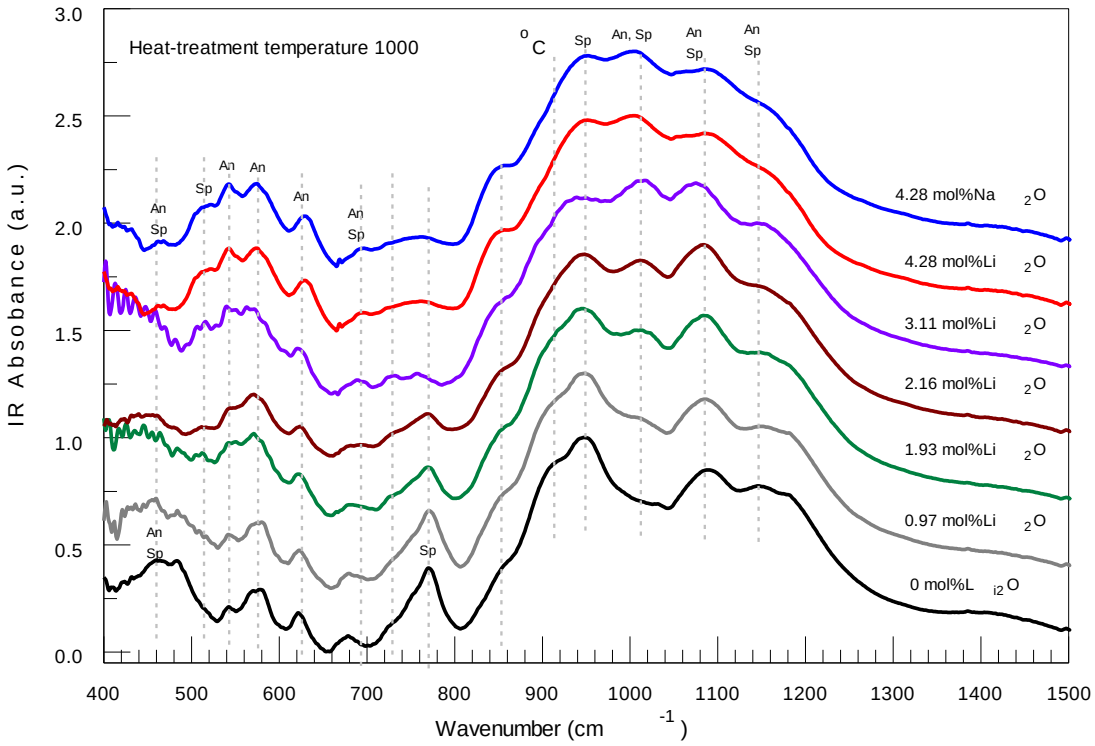

Fig. S1 IR spectra of the MCAS glasses heat-treated at 1000^{o}C for 20h (Spectra are vertically shifted for better clarity, An-anorthite, Sp-spodumene).

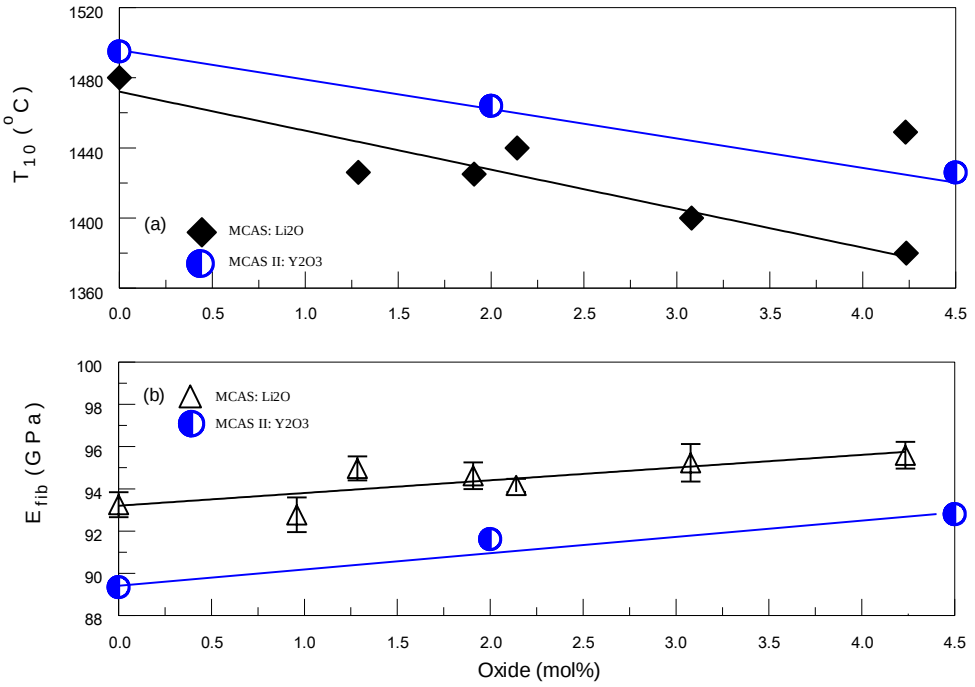

Fig. S2 Effect of Li_2O and Y_2O_3 on (a) glass melting temperature (T_{10}) and (b) fiber sonic modulus (E_{fib})

Other references may be considered (TBD)

[] Gallo LSA, Mosca TDM, Teider BH, Polyakova I, Rodrigues ACM, E.D. Zanoto ED, Fokin VM. Effects of lithium on the crystallization kinetics of $Na_2O•2CaO•3SiO_2$ glass. *J. Non-Cryst. Solids*. **2015**; 408:102-114.

[21] Abel BM, et. al. Liquidus surface of MgO-CaO-Al_2O_3-SiO_2 glass-forming systems. *J. Non Cryst. Solids*. **2013**, 363:39-45.

O.N. Koroleva, "The structure of lithium silicate melts revealed by high-temperature Raman spectroscopy," Spec. Lett. 50 (2017) 257-264.

[11] Demirok G, Atilgan S, Li, H. Raman spectroscopic study and statistical modeling of composition-structure-property of MgO-CaO-Al_2O_3-SiO_2 based glasses. *J. Non-Cryst. Solids.* 2024, 626:122787.

[28] Li H, Demirok G. Natural silicates in glass fiber production. Glass Technol.: J. Eur. Glass Sci. Technol. Part A. (in print, 2024).

[29] Sardisco L, Hannula P-M, Pearce TJ, Morgan L. Multi-technique analytical approach to quantitative analysis of spodumene. Minerals. 2022, 12: 175

[30] Sharma SK, Mammone JF, Nicol MF. Raman investigation of ring configurations in vitreous silica. *Nature*. 1981, 292: 140-141.

Daniel R. Neuville, Viscosity, structure and mixing in (Ca, Na) silicate melts

[34] Neuville DR, Cormier L, Massiot D. Al coordination and speciation in calcium aluminosilicate glasses: effects of composition determined by ^{27}Al MQ-MAS NMR and Raman spectroscopy. *Chem. Geology*. **2006**, 229: 173-185.

[35] McMillan P, Piriou B. Raman spectroscopy of calcium aluminate glasses and crystals. *J. Non-Cryst. Solids.* **1983**, 55: 221-242.

[35] Neuville DR. Viscosity, structure and mixing in (Ca, Na) silicate melts. *Chem. Geology*. **2006**, 229: 28-41.